ACOUSTICS 2012

Acoustic properties of perforated plates and screens

H.L. Ruiz Villamil[a], P. Cobo[a], T. Dupont[b] and P. Leclaire[b]

[a]Centro de Acústica Aplicada y Evaluación no Destructiva, Calle Serrano 144, 28006 Madrid, Spain
[b]LRMA-DRIVE, ISAT, 49 rue Mademoiselle Bourgeois - BP 31, 58027 Nevers, France
thomas.dupont@u-bourgogne.fr

In previous works, an acoustic model for Microperforated Insertion Unit (MIU), was developed to determine the input impedance of a system composed of a thin mesh (or screen) glued onto a perforated plate. An alternative approach is proposed by means of the equivalent fluid model of Johnson-Champoux-Allard involving five physical parameters: the tortuosity, the thermal and viscous characteristic lengths, the porosity and the flow resistivity. The input impedance of a multiple layer system can then be found by use of the transfer matrix method. Since the meshes have fairly simple structures, it was possible to model an elementary representative cell and to use calculated values for the five parameters. The resistivity was also evaluated from absorption measurement for the screen alone in an impedance tube. For the thermal and viscous characteristic lengths, the calculated values were also compared to measurements obtained from a microscope image of the elementary cells of the screen. A hybrid model using the theory by Maa for the perforated plate and the theory by Johnson-Champoux–Allard for the micrometric mesh was developed. This model is in very good agreement with experimental results.

1 Introduction

In the early 1970's Maa[1] proposed an analytical model to predict the acoustic impedance of a microperforated panel (MPP) combining the model of sound propagation in narrow tubes studied by Crandall and Rayleigh [2, 3] and the end corrections proposed by Ingard [4]. Maa recommended to design panels with a diameter of perforation – to – thickness ratio close to one to obtain optimal absorption properties.

Drilling submillimetric holes in a panel can be an expensive and difficult task. However, using slits, the manufacturing can be less expensive and the amount of perforations can be reduced keeping the porosity equal to that of an MPP [5, 6].

In some cases, a perforated plate can also be modelled as a rigid frame porous medium described by the Johnson-Champoux-Allard (JCA) theory [7, 8, 9] that depends on five physical parameters: the porosity ϕ, the tortuosityα_∞, the thermal Λ' and viscous Λ characteristic lengths and the static air flow resistivity σ. Atalla and Sgard [10] presented an equivalent fluid approach considering these parameters. The approaches in references [1], [5] and [10] agree in what concerns the impedance inside the perforations but the end corrections differ. While Atalla and Sgard [10] introduce the end correction by means of the geometric tortuosity α_∞, Maa[1, 5] introduces the end correction as an additional complex impedance with resistive and reactive components.

Combining a carrying plate with a porous material or textile [11, 12, 13] the sound attenuation can be increased. Using the impedance transfer method [14], Pfretzschner et al. [12] proposed a combination of a perforated panel and a micrometric mesh, which they named a microperforated insertion unit (MIU). The impedance of the MIU results from the addition of the acoustic impedances of the perforated plate and of the mesh divided by the open area fraction of the plateϕ.

In this study, multilayer systems made of macroperforated metal plates backed by microperforated woven meshes are considered. This configuration can significantly decrease the costs of manufacturing an acoustic system. A precise estimation of the thermal characteristic length involving a simple model for the elementary cell of the woven textile structure and a hybrid model designed for non-homogenously distributed macroperforated panels backed by woven textiles are proposed. The analytical approach of Maa [1, 5] is used to model the circular or slit-like macro perforated carrying plates whereas the JCA model is used in the rigid frame approximation for the mesh. In the hybrid model, the distribution of the perforations over the surface of a carrying plate does not matter [15].

An effective resistivity is introduced to account for a diaphragm effect between the carrying plate and the mesh. The flow resistivity of the mesh is calculated by means of the shape factor described by Stinson and Champoux [16]. The theory used to obtain the impedance of the carrying plate is presented in section 2. The calculation of the thermal characteristic length of microperforated woven meshes is described in section 3. Section 4 presents the derivation of the effective flow-resistivity and the hybrid model using a combination of the models of Maa and JCA in the context of the transfer matrix method. Experimental validation is presented in the last section.

2 Impedance of a microperforated plate

The surface impedance of a perforated panel can be written as the sum of two contributions [1, 5]: the impedance at the borders which accounts for the end corrections and the impedance at the interior of the perforation:

$$Z_1 = \frac{\sqrt{2}\mu y}{\phi d} + \frac{j\omega\rho_0}{\phi}\left[R\psi(\xi)r + \frac{t}{[1-S]}\right], \quad (1)$$

where ρ_0 is the air density, μ the air kinematic viscosity coefficient, ω the angular frequency, r the perforation radius, t the panel thickness, ϕ the perforation ratio and $y = d/\sqrt{4\mu/\rho_0\omega}$ with d the perforation diameter R and S are parameters that depend on the geometry of the perforations, in particular on the length of the slit l. In the case of periodic hole arrangement, $\psi(\xi)$ is a correction of the reactance term of the end correction that takes into account the interaction between holes when the perforation ratio is high [17, 18].

$$\begin{aligned}\psi(\xi) = 1 - 1.4092(\xi) + 0.33818(\xi)^3 \\ + 0.06791(\xi)^5 - 0.02287(\xi)^6 \\ + 0.03015(\xi)^7 - 0.01641(\xi)^8\end{aligned} \quad (2)$$

where $\xi = 0.88\frac{d}{b}$. The end corrections studied by Rayleigh and Ingard [2, 4] are included in the first and second term of Eq. (1). The numerator of the second term accounts for the influence of a mass of air contained in a cylindrical volume for which the apparent length is greater than the plate thickness. The impedance of the perforations which has been studied by Crandall [3] for an array of tubes and by Ingard [4] for an elliptic aperture, is included in the

third term. The velocity profile of the flow through the holes is determined by the term y. Table 1 shows the values of R and S where J_0, J_1 are Bessel functions of the first kind and order 0 and 1, respectively and $F_{(e)}$ is an elliptic integral with $e = \sqrt{1-(r/l)^2}$.

$$F_{(e)} = \frac{\pi}{2}\left[1 + \left(\frac{1}{2}\right)^2 e^2 + \left(\frac{1\times 3}{2\times 4}\right)^2 e^4 + \left(\frac{1\times 3\times 5}{2\times 4\times 6}\right)^2 e^6 + \cdots\right], \quad (3)$$

Table 1.Values of R and S for different carrying plates.

Type of perforation	R	S
Circular	1.7	$\frac{2}{y\sqrt{-j}}\frac{J_1 y\sqrt{-j}}{J_0 y\sqrt{-j}}$
Slit	$F_{(e)}$	$\frac{\tanh\left(y\sqrt{j}\right)}{y\sqrt{j}}$

3 The micrometric mesh as an equivalent fluid

3.1 Parameter characterization

Atalla and Sgard considered a plate or screen as an equivalent fluid using the rigid frame porous model developed by Johnson-Champoux-Allard [7, 8, 9]. In the equivalent fluid approach, the end corrections are introduced by means of the tortuosity allowing to define the boundary conditions in multilayer configurations. Latest works apply this model for woven or non-woven fabrics [13, 19]. In many cases, a cylindrical cross section of perforations is considered. Nevertheless, as the woven meshes studied here exhibit more complex pore geometries, a three dimensions approach is needed.

In the JCA model, the tortuosity, resistivity, porosity and characteristic lengths of the pores can be obtained [8] or measured for each specific equivalent fluid. The visco-thermal effects associated with a wave impinging onto a porous medium can be modelled introducing a complex dynamic density i.e, the effective density $\tilde{\rho}_e(\omega)$ (see ref. 7)

$$\tilde{\rho}_e(\omega) = \alpha_\infty \rho_0 \left(1 + \frac{\sigma\phi}{j\omega\rho_0\alpha_\infty}\sqrt{1 + \frac{j\omega 4\alpha_\infty{}^2\mu\rho_0}{\sigma^2\Lambda^2\phi^2}}\right), \quad (4)$$

where α_∞ is the tortuosity, ρ_0 the air density, σ the flow resistivity, $\phi$the porosity, which is considered equivalent to the perforation ratio, ω the angular frequency, μ is the air kinematic viscosity coefficient and Λ is the viscous length given by [8]

$$\frac{2}{\Lambda} = \frac{\int_S v_i^2(r_w)dS}{\int_V v_i^2(r)dV}. \quad (5)$$

The integrations of the numerator and the denominator of Eq. (4) are over the walls of the pore perforation and over the pore volume, respectively.

The parameters α_∞ and σ are important factors in the calculation of the effective density. While the tortuosity depends on the pore shape and the layer arrangement, the flow resistivity depends on the pore shape. For a screen with air at both sides, $\alpha_\infty = 1 + (2\varepsilon/t)$, where ε represents a correction length.

The equivalent fluid MPP's approach [10] and the classical MPP's formulation [1] take into account the increase of kinetic energy caused by the sound radiation effect at the end openings of perforations and the distortion effect of the acoustic flow at the panel surface. As a result, the MPP's reactance must be supplemented by an additional mass by way of the length correction ε on the plate thickness, in the imaginary part of the MPP's impedance [4, 7]. In the case of a single perforation, the classical approach employs an analogy with the radiation impedance of a rigid piston with a circular cross section flanged in an infinite rigid wall. For this approach the end termination of perforation is considered to have a sharp edge. In the present study, however, the end termination of the screen perforation has rounded edges. This kind of edge tends to diminish the length correction [20]. Moreover, when there are several perforations in close proximity, one must consider that the interaction between perforations tends to diminish the length correction [4, 6]. For the meshes treated in this study, the flange between two perforations is small compared to their size, which causes a strong interaction between the rounded edges of the pore. The length correction is thought to be very small and is therefore disregarded. As a result, the effective tortuosity is equal to 1.

The flow resistivity σ has been described by Stinson and Champoux [16] for simple pore shapes as

$$\sigma = \frac{4k_0\mu\alpha_\infty{}^2}{h_r{}^2\phi}, \quad (6)$$

where, h_r is the hydraulic radius and k_0 is a constant parameter for a given pore shape. When the perforations are assumed of cylindrical shape with constant cross section, the viscous characteristic length and the thermal characteristic length are equal to the hydraulic radius of the perforation [7, 10, 13, 19] $\Lambda = \Lambda' = h_r = d/2$. However as will be seen in the next section, this assumption cannot be made for other pore geometries.

Considering woven membranes as materials with identical uniform pores, the effective density can be linked to the dynamic bulk modulus given by [7, 9]

$$K(\omega) = \frac{\gamma P_0}{\gamma - (\gamma-1)(1 + H\sqrt{1 + j\omega/H}/j2\omega)}, \quad (7)$$

where γ is the fluid specific heat ratio, P_0 is the fluid equilibrium pressure, ω the angular frequency and $H = 16\mu/\left(N_{Pr}\Lambda'^2\rho_0\right)$. N_{Pr} is the Prandtl number. The thermal length Λ' characterizes the high frequency behavior of the bulk modulus[9]. A simple model to calculate Λ' is presented in section 3.2. Equations (4) and (7) allow to calculate the characteristic impedance Z_c of the fluid,

$$Z_c = \sqrt{K(\omega)/\tilde{\rho}_e(\omega)}, \quad (8)$$

and the associated wave number

$$k = \omega\sqrt{\tilde{\rho}_e(\omega)/K(\omega)}. \quad (9)$$

3.2 Simple model for calculating the thermal length of woven meshes

The thermal characteristic length is defined as the surface to pore volume ratio of the pore solid interface [9]

$$\frac{2}{\Lambda'} = \frac{\int_S dS}{\int_V dV} = \frac{S}{V}. \quad (10)$$

Assuming isotropic meshes with cylindrical yarns, an original model to obtain the thermal length is proposed. The elementary cell of the screen perforation is shown in Fig. 1.

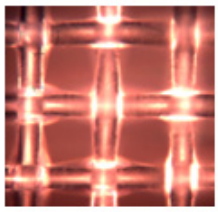

Figure 1.Microscopic image of an elementary cell of a woven mesh.

The volume of air passing through the pore depends on the end termination of the yarn geometry. A simple calculation can be made by observing a single perforation as the one in Figure 2a. The volume of air through the cell is observed in Figure 2b.The volume of each truncated cylinder in the elementary cell of Figure 2a is

$$V_h = \pi {r_y}^2 b - 4\int_{-r_y}^{r_y}\int_0^{\sqrt{{r_y}^2-x^2}} y\,dx\,dy, \quad (11)$$

where r_y is the yarn radius and $b = d + 2r_y$. The volume V_p of the pore (Figure 2b) is then

$$V_p = b^2 Y_d - \frac{4V_h}{2}. \quad (12)$$

Figure 2b represents Eq. (12). The surface of each truncated cylinder is

$$S_h = 2\pi r_y b - 4\int_0^{\pi} {r_y}^2 sin\theta d\theta. \quad (13)$$

The interior surface S_p of the pore is then

$$S_p = \frac{4S_h}{2}. \quad (14)$$

The thermal length can be obtained replacing S_p in S and V_p in V in Eq. (10)

$$\Lambda' = \frac{b^2 - b\pi r_y + (8/3{r_y}^2)}{\pi b - 4r_y}. \quad (15)$$

In the examples studied, it is found that the thermal characteristic length calculated via Eq. (15) can be smaller than the viscous characteristic length. This result tends to show that for the microstructure studied, the thermal effect can have a large influence on the bulk modulus at high frequencies.

Assuming identical square pores for the particular geometry of a woven mesh, the physical parameters are: $\Lambda = r$, $\alpha_\infty = 1$, σ is obtained with Eq. (6) where[16]$k_0 = 1.78$, Λ' is obtained with Eq. (15) and $\phi = (d/(Y_d + d))^2$.

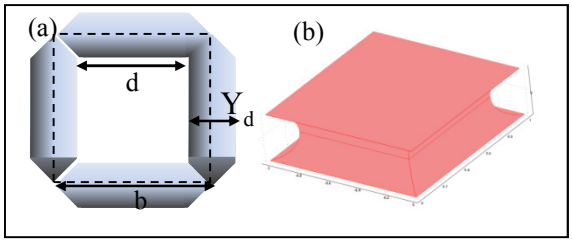

Figure 2. Simple model for a single mesh perforation geometry. a) fiber structure (the dotted rectangle represents the elementary cell), b) inside volume.

4 A hybrid model in the transfer matrix context

In the present work, the transfer matrix approach [7] is used to obtain the impedance of a system composed of a perforated plate carrying a micrometric mesh and the acoustic impedance of the whole system is obtained considering the impedance matrix of each element. A hybrid model combining the Maa model for the macro-perforated plate and the JCA model for the micrometric mesh is proposed to obtain the input impedance of a multiple layer system.

The absorption curve of the hybrid model Maa-JCA depends on 7 parameters (d_1,t_1,ϕ_1,d_2,t_2,ϕ_2,D), where d_1,t_1,ϕ_1,d_2,t_2,ϕ_2 are the pore diameter, thickness and porosity of the carrying plate and the mesh respectively, and D is the air cavity thickness. Using the impedance provided by Maa (Eq. (1)), the impedance matrix for a carrying plate with circular or slits perforations can be obtained as

$$T_{Plate} = \begin{bmatrix} 1 & j(imag(Z_1)) \\ 0 & 1 \end{bmatrix}. \quad (16)$$

In this study, carrying plates with perforations sizes greater than 1 mm and perforations rates close to 10 % are considered, the viscous characteristic frequency is very low, so the thermo-viscous effect can be disregarded [7]; however, the mass effect is very high. As a consequence the impedance expression can be reduced in such a way that only the imaginary part is taken into account. Indeed, the experimental sound absorption coefficient of this plate (MPP or MSP without screen) coupled with an air cavity and rigid wall is weak.

The matrix for an equivalent fluid i.e. the mesh or the air cavity, is given by

$$T_{Eq} = \begin{bmatrix} \cos(k_{Eq}t_{Eq}) & \frac{jZ_{cEq}\sin(k_{Eq}t_{Eq})}{\phi_f} \\ \phi_{Eq}Z_{cEq}\sin(k_{Eq}t_{Eq}) & \cos(k_{Eq}t_{Eq}) \end{bmatrix}, \quad (17)$$

Where $t_{Eq}, \phi_{Eq}, Z_{cEq}, k_{Eq}$ are the thickness, the porosity, the characteristic impedance and the wave number of the fluid. For example if the equivalent fluid is the air cavity, $t_{Eq}, \phi_{Eq}, Z_{cEq}, k_{Eq}$ are replaced by the properties of air i.e. D, 1, Z_{cAir}, k_{Air}. Eq. (8) and (9) allow to obtain Z_{cM}, k_M respectively.

A transfer matrix can be adapted for each new layer of plate, mesh or air. The multilayer configuration is obtained with Eq. (21). Figure 3 shows the effect of the flow inside the perforations. The particle velocity is the same at both

sides of the hybrid system. The particle velocity inside the pores is always greater than outside them because ϕ_1 and ϕ_2 are always smaller than 1.

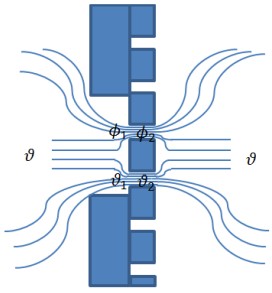

Figure 3. Viscous flow of the fluid through the perforations.

The course of the flow in the woven mesh and the relationship between the pressure gradient ΔP and the particle velocity are described by Darcy's law:

$$\Delta P = -\phi \vartheta \sigma. \quad (18)$$

A "diaphragm effect" is observed in Fig. 3 when a macro perforated plate is coupled with a mesh without airspace between the two elements and therefore a correction should be incorporated to Darcy's law. The flow velocity at the entrance of the pores of the mesh is increased as the flow is squeezed inside the plate macroperforations. To account for this phenomenon the flow resistivity of the mesh should be modified by a correction factor which is precisely the porosity of the carrying plate. As a result, the resistivity of the mesh should be replaced by an "effective resistivity" of the combination plate-mesh

$$\sigma_{eff} = \frac{\sigma_{mesh}}{\phi_{Plate}}. \quad (19)$$

Therefore the modified Darcy law for the mesh is

$$\Delta P = -\phi_{mesh} \vartheta_{mesh} \sigma_{eff}. \quad (20)$$

The multiplication of the individual matrices results in the global transfer matrix of the hybrid model:

$$T_{hybrid} = [T_{Plate}][T_{Eq\_Mesh}][T_{Eq\_Air}]. \quad (21)$$

The input impedance of the system and absorption coefficient are then obtained by

$$Z_h = \frac{T_{11}^h}{T_{21}^h}, \alpha = 1 - \left|\frac{Z_h - Z_0}{Z_h + Z_0}\right|^2. \quad (22,23)$$

5 Results and discussions

In this section, the hybrid model and the validity of the approaches used to evaluate Λ' and σ are tested. The experiments were carried out in a laboratory where the atmospheric conditions were: T=23ºC, Po=103070 Pa, c=344.9m/s, ρ_0=1.21 kg/m^3, $\mu = 1.83 \times 10^{-5}$ Kg m^{-1}s^{-1}, γ =1.4 and N_{pr}= 0.71.Four different macro-perforated panels where used as carrying plates for five precision and non-precision woven meshes.

Figure 4 shows the absorption curve of a commercial woven mesh placed in front of a rigid wall *(d,t,ϕ,Y_d,D)=(36 μm,50 μm,28 %,33 μm, 5cm),*where d is the diameter of perforations, t the thickness, ϕ the perforation ratio, Y_d the yarn diameter and D the air cavity thickness. A good agreement between the JCA model and the measurement is achieved. For this example, the manufacturer´s nominal parameters were used and good results were obtained.

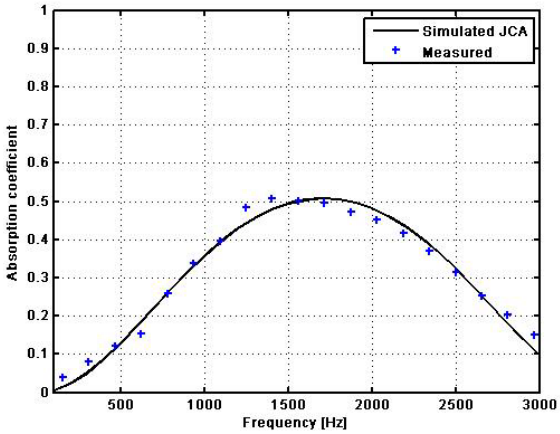

Figure 4. Absorption curve of a mesh with parameters (*d, t, p, Y_d, D*)=(36 μm,50 μm,28 %,33 μm, 5cm).

The experimental validation of the hybrid model is now proposed. The four macro-perforated carrying plates with d = 3, ϕ = 9.96 % and t = 1 mm are shown in Figure 5. While in plate 3 the hydraulic diameter is equal $\text{tor}_h = \Lambda = d/2$, in plates 1, 2 and 4 is it equal $\text{tor}_h = \Lambda' = \frac{ld}{l+d}$. A good adjustment is obtained for ξ = 0.25, 0.25, 0.35 and 0.28 for plates 1 to 4 respectively. Non-precision woven (meshes *a* and *d*) and precision woven meshes (meshes *b*, *c* and *e*) where tested (see Figure 6).

The pores and yarn diameter were obtained using the software Optika vision lite and an Euromex Holland microscope.

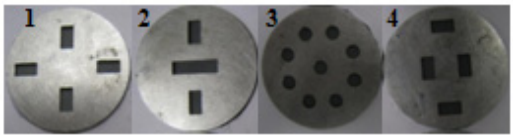

Figure 5. MPPs and MSPs with different perforations distribution.

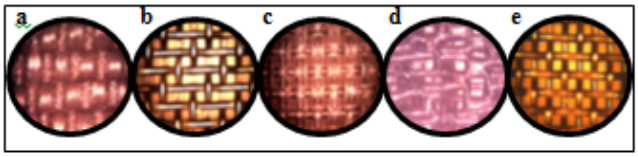

Figure 6. Microscopic image of the meshes tested a)Woven screen, b) sefar® acoustic BHY, c) sefar® Nitex 41/31, d) curtain e) sefar® acoustic HF 34-39.

The microscopic analysis allowed to calculate the viscous and thermal characteristic lengths. The thickness was measured with a digital caliper. The porosity was also evaluated by the expression $\phi = (d/(Y_d + d))^2$. The precision on the evaluation of the porosity when compared to the manufacturer's value was 5%.

It is seen that when $Y_d \geq 3.3d$, the thermal length calculated by Eq. (15) is smaller than the viscous length taken to be equal to half the interfiber distance d. This is the case for all the meshes studied except for mesh *a*.

Figure 7 illustrates the results of combining plate 1 with meshes *a*, *b* and *d*. Two interesting results are highlighted. First, the hybrid model presents a very good agreement with the experimental measurements for precision woven and non-precision woven meshes. Second, a very high absorption is achieved by using mesh *b* and *d* and while the first one is a commercial precision woven mesh used for filtering, the second one is a simple woven curtain. The difference in costs between the two meshes is about 10 times and the results are very similar. The model was also validated for a carrying plate with circular perforations. It appears that using the same mesh with two different plates with the same perforation ratio but different perforations distribution provides very similar absorption curve.

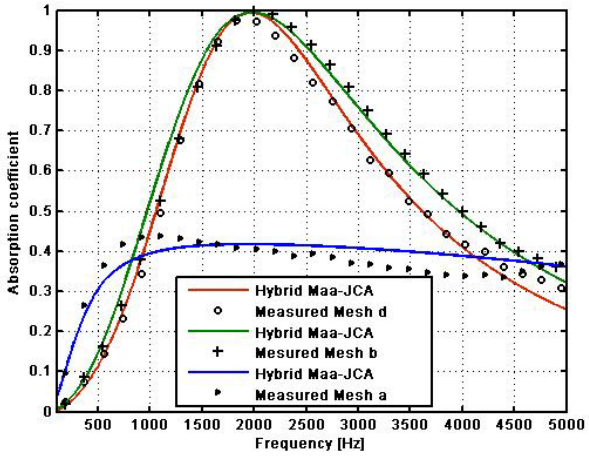

Figure 7. Absorption curve of plate 1 combined with mesh a (>), b (+), and d (o). Air cavity D=2cm.

5 Conclusion

In this work, a hybrid acoustic model using a macro perforated carrying plate and a micrometric woven mesh has been proposed. A simple equation for the calculation of the thermal characteristic length with square pores was used. It is found that in the woven mesh geometries studied, the thermal characteristic length can be smaller than the viscous characteristic length. This result tends to show that the thermal effects have a great importance in woven meshes at high frequencies. To account for a "diaphragm effect" due to the squeezing of the air flow inside the macroperforation into the mesh was proposed. This results in an effective flow resistivity for the mesh. The transfer matrix method allows to handle multilayer configurations. The macroperforated plate can be studied in the framework of the classical Maa model while the porous layer can be modelled as an equivalent fluid with the JCA approach.

Acknowledgments

This work has been supported by the Spanish Ministry of Science and Innovation (MICINN) through Project TRA2011-26261-C04-01.

References

[1] D. Y. Maa, "Microperforated-panel wideband absorbers", *Noise Control Eng. J.* 29, 77–84 (1987)

[2] J. B. Crandall, *Theory of vibrating systems and sound*, Van Nostrand, New York, (1926)

[3] J. W. S. Rayleigh, *The Theory of sound*, MacMillan, London, (1926)

[4] U. Ingard, "On the theory and design on acoustic resonators", *J. Acoust. Soc. Am.* 25(6), 1037–1061 (1953)

[5] D. Y. Maa, "Theory of microslit absorbers (in chinese)", *Acta Acustica* 25, 481–485 (2000)

[6] R. Randeberg, "Perforated panel absorbers with viscous energy dissipation enhanced by orifice design," Ph.D. dissertation, Norwegian University of Science and Technology, Trondheim (2000)

[7] J. Allard and N. Atalla, *Propagation of Sound in Porous Media. Modelling Sound Absorbing Materials*, Wiley, Chichester, United Kingdom (2009)

[8] J. K. D.L. Johnson and R. Dashen, "Theory of dynamic permeability and tortuosity in fluid-saturated porous media", *J. Fluid Mech.* 176, 379–402 (1987)

[9] Y. Champoux and J. Allard, "Dynamic tortuosity and bulk modulus in air-saturated porous media", *J. Appl. Phys.* 70 (1), 975–1979 (1991)

[10] N. Atalla and F. Sgard, "Modeling of perforated plates and screens using rigid frame porous models", *J. Sound Vib*. 303, 195–208 (2007)

[11] J. Kang and H. V. Fuchs, "Predicting the absorption of open weave textiles and micro-perforated membranes backed by an air space", *J. Sound Vib*. 220, 905–920 (1999)

[12] J. Pfretzschner, P. Cobo, F. Simon, M. Cuesta, and A. Fernández, "Microperforated insertion units: an alternative strategy the design of microperforated panels", *Appl. Acoust*. 67, 62–73 (2006)

[13] F. Chevillote, "Controlling sound absorption by an upstream resistive layer", *Appl. Acous.* 73(1), 56–60 (2012)

[14] P. Cobo, M. Cuesta, and M. Siguero, "Comparison of models describing double layer microperforated absorbers", *Noise Control Eng. J.* 57, 10–15 (2009)

[15] H. Ruiz and P. Cobo, "Proposal of alternative designs for microperforated panels" in Proceedings of the 40th International Congress and Exposition on Noise Control Engineering, Internoise. Osaka, Japon, September 4-7 (2011)

[16] M. Stinson and Y. Champoux, "Propagation of sound and the assignment of shape factors in model porous materials having simple pore geometries" *J. Acoust. Soc. Am.* 91(2), 685–695 (1992)

[17] T. H. Melling, "The acoustic impedance of perforates at medium and high sound pressure levels", *J. Sound Vib.* 125, 1–65 (1973)

[18] R. Tayong, T. Dupont, and P. Leclaire, "Experimental investigation of holes interaction effect on the sound absorption coefficient of micro-perforated panels under high and medium sound levels", *App. Acous*. 72, 777–784 (2011)

[19] L. Jaouen and F.-X. Bécot, "Acoustical characterization of perforated facings", *J. Acoust. Soc. Am.* 129(3), 1400–1406 (2011)

[20] J. P. Dalmont, C. J. Neverveen, and N. Joly, "Radiation of tubes with different flanges: numerical and experimental investigations", *J. Sound Vib*. 244(3), 505–534 (2001)